Study of the magnetite to maghemite transition using microwave permittivity and permeability measurements

2016 J. Phys.: Condens. Matter 28 106002

(http://iopscience.iop.org/0953-8984/28/10/106002)

OPEN ACCESS
IOP Publishing
Journal of Physics: Condensed Matter
J. Phys.: Condens. Matter **28** (2016) 106002 (10pp)
doi:10.1088/0953-8984/28/10/106002

Study of the magnetite to maghemite transition using microwave permittivity and permeability measurements

Jerome Alexander Cuenca[1], Keith Bugler[3], Stuart Taylor[3], David Morgan[3], Paul Williams[1], Johann Bauer[4] and Adrian Porch[2]

[1] Cardiff Wolfson Centre for Magnetics, School of Engineering, Cardiff University, Cardiff, CF24 3AA, UK
[2] Centre for High Frequency Engineering, School of Engineering, Cardiff University, Cardiff, CF24 3AA, Wales, UK
[3] Cardiff Catalysis Institute, School of Chemistry, Cardiff University, Cardiff, CF10 3AT, Wales, UK
[4] Research and Development Pigments and Cosmetics, Merck KGaA, Darmstadt, 64293, Germany

E-mail: cuencaj@cardiff.ac.uk

Received 10 November 2015, revised 18 December 2015
Accepted for publication 22 December 2015
Published 16 February 2016

Abstract

The microwave cavity perturbation (MCP) technique is used to identify the transition from magnetite (Fe_3O_4) to the meta-stable form of maghemite (γ-Fe_2O_3). In this study Fe_3O_4 was annealed at temperatures from 60 to 300 °C to vary the oxidation. Subsequent to annealing, the complex permittivity and magnetic permeability of the iron oxide powders were measured. The transition to γ-Fe_2O_3 was corroborated with x-ray diffraction (XRD), x-ray photoelectron spectroscopy (XPS) and vibrating sample magnetometry (VSM). XRD, XPS and VSM implied that the starting powder was consistent with Fe_3O_4 and the powders annealed at more than 200 °C were transitioning to γ-Fe_2O_3. The MCP measurements gave large differences in both complex permittivity and magnetic permeability of the two phases in the frequency range of 2.5–10.2 GHz. Magnetic permeability decreased with annealing temperature, though magnetic losses showed frequency dependent behaviour. Complex permittivity measurements showed a large decrease in both dielectric constant and losses at all measurement frequencies, as well as a prominent loss peak centred around the phase transition temperatures. We interpret the loss peak as being a consequence of field effects due to an intermediate multi-phase mixture. Additionally, almost no frequency dependence was observed. The reduction in complex permittivity implies that the Fe^{2+}_{oct} cations in the lattice provide a significant contribution to polarization at microwave frequencies and the effects of Fe^{3+}_{oct} are nominal in comparison. The change in loss can be explained as a combination of the differences in the effective conductivity of the two phases (i.e. Fe_3O_4 exhibits electron-hopping conduction whereas the presence of vacancies in γ-Fe_2O_3 nullifies this). This shows that the non-invasive MCP measurements serve as a highly sensitive and versatile method for looking at this phase transition in iron and potentially the effects of oxidation states on the polarization in other iron oxides.

Keywords: magnetite transition, maghemite determination, complex permittivity, complex permeability, microwave cavity perturbation, electron hopping conduction

S Online supplementary data available from stacks.iop.org/JPhysCM/28/106002/mmedia

(Some figures may appear in colour only in the online journal)

I. Introduction

Magnetic particles have gained great interest recently in applications ranging from electromagnetic absorbers [1–4] to numerous biomedical applications including magnetic drug delivery [5] and treatment of hyperthermia [6, 7]. In particular, magnetite (Fe_3O_4) and maghemite (γ-Fe_2O_3) have been highlighted as suitable candidates for these applications due to the simplicity of their synthesis, biocompatibility and non-toxicity [8, 9]. Fe_3O_4 can be synthesized through coprecipitation of iron salts. Synthesis of γ-Fe_2O_3 is most commonly through subsequent oxidation of Fe_3O_4, with the exception of the dehydroxylation of iron oxide-hydroxides such as lepidocrocite (γ-FeOOH) or goethite (α-FeOOH) [10, 11]. Oxidation of Fe_3O_4 in air at temperatures around 200–300 °C induces the phase change to γ-Fe_2O_3 [12–14]. These two oxides are of interest due to their structural similarity but γ-Fe_2O_3 is the more thermally and chemically stable of the two [15, 16].

Current standard techniques to study the synthesis of γ-Fe_2O_3 include x-ray diffraction (XRD) [17, 18], x-ray spectroscopy (XPS), x-ray absorption near edge spectroscopy (XANES) [19], vibrating sample magnetometry (VSM), Raman and IR spectroscopy [20, 21], and Mössbauer spectroscopy [12, 22]. The most effective method is Mössbauer spectroscopy since it specifically probes the oxidation state of the irons from the sextet caused by Zeeman splitting from the different nuclear spin moments. XRD works by changes in lattice constant but since both oxides have the same inverse spinel lattice, identifying γ-Fe_2O_3 after oxidation is by no means trivial. The lattice constant of γ-Fe_2O_3 (8.34 Å) is slightly smaller than Fe_3O_4 (8.39 Å), resulting in a shifted diffraction pattern towards smaller angles for Fe_3O_4 when compared with γ-Fe_2O_3. A difference can be identified though from the shift in the (5 1 1) plane [23]. For a multi-phase material, a convolution of two peaks with intensities dependent upon the concentrations of Fe_3O_4 and γ-Fe_2O_3 can be seen. XPS probes a difference in binding energy of the Fe 2p core electrons, as well as characteristic satellite peaks caused by particular oxidation states in materials. This technique is a very effective surface probe, but is less sensitive to the bulk. Raman Spectroscopy is able to identify the material phases through distinct differences in phonon scattering of the A_{1g}, E_g and T_{2g} modes [20, 21]. However, due to the nature of the measurement it can induce the phase change to hematite, caused by heating from the laser and thus great care must be taken to measure these materials [21, 24, 25]. Though phase identification can be achieved, there are some drawbacks to all of these methods, including complicated analysis, low sensitivity, invasive (to the point of destruction) and the demand for complex, expensive experiments which sometimes involve ionizing radiation.

Since the process is related to cations with unpaired electron spins, polarization (via permittivity) and permeability measurements may offer a complementary insight to the transformation. This can be achieved through impedance spectroscopy and magnetometry [26]. For the former this requires powdered samples to be compressed, shaped and physically built into the measurement system. Though this method infers the conductivity, repeatability becomes a problem as well as system contamination due to contact. For magnetic measurements, high precision field probes with large magnets or superconducting detectors require controlled cooling to support large fields. Our present study explores whether the conversion of Fe_3O_4 to γ-Fe_2O_3 can be observed using non-invasive dielectric and magnetic probing techniques, in particular MCP. The MCP approach may offer a simpler and highly sensitive measurement system for oxidation analysis, which could be applied to many other materials systems apart from iron oxides.

II. Principles of microwave characterization

Microwave cavity perturbation (MCP) provides a non-contacting electromagnetic probe through the simple perturbation of high density fields as opposed to contact measurements at DC (or low frequencies) and subsequent measurement of impedance through voltage and current. In MCP, the powder of interest is simply poured into a low microwave loss container and placed into the antinode of the appropriate standing wave (electric or magnetic) of a microwave cavity resonator. The greatest advantages of this approach are the non-contact nature of the measurement, as well as low power requirements (generally it uses input power levels of approximately 1 mW, with typically less than 10 μW dissipated in the sample). Microwave systems have been explored to measure some iron oxides through electron spin resonance (ESR) where a sample perturbs a microwave cavity resonator whilst subject to a DC magnetic field (often modulated by Helmholtz coils to increase the signal to noise ratio using lock-in amplifiers). The DC field aligns the electron spins parallel and anti-parallel, creating Zeeman splitting where the equivalent energy level difference lies in the microwave region through the Einstein relation $E = hf$. Maximum absorption occurs when the microwave frequency of the resonator matches that of the energy difference E. It has been shown that Fe_3O_4 and γ-Fe_2O_3 give different ESR responses, with γ-Fe_2O_3 giving a narrower linewidth at absorption [27–29]. If the differences in the materials' properties can be expressed in a simple change in cavity resonance alone, there is no need for the additional instrumentation imposed by ESR. Hence we move from probing spin resonance to simple bulk complex permittivity and permeability measurements, which eliminates the need for a large DC electromagnet, field calibration procedures and other added complexities, reducing the system to just a resonator and a means of interrogating it. Whilst we use a vector network analyser for the measurements presented here, a simple system involving a voltage controlled oscillator and a power detector will suffice.

Complex permittivity (hence conductivity) and permeability measurements using MCP are very simple. The sample is placed inside a hollow metal cavity and the differences that arise in complex resonant frequency between the unperturbed and sample perturbed states (the real part being centre frequency and imaginary part being related to the quality factor,

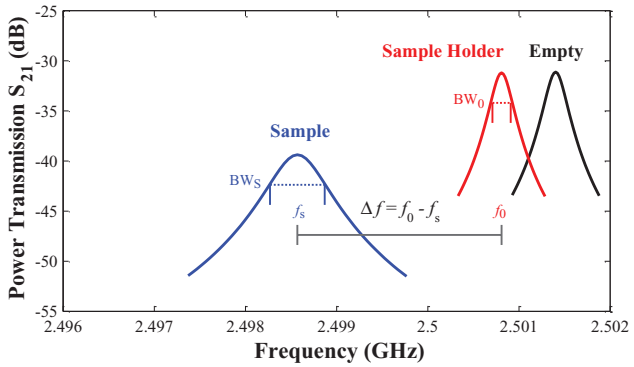

Figure 1. Example of resonant traces from an MCP measurement. The procedure involves measuring the frequency and 3 dB bandwidth (BW) of the unperturbed state denoted by '0' and the sample perturbed state denoted by '*s*'. These values can be related to real and imaginary parts of the complex permittivity or permeability.

full-width half maximum or 3 dB bandwidth, see figure 1). The sample can be placed into either an electric or magnetic field maximum to measure the microwave permittivity or permeability, respectively, at that resonant frequency. Different standing wave patterns are created at different resonant frequencies depending upon the geometry and the materials used to construct it. For a cylindrical cavity resonator, these are given by the well-known resonant frequency equation:

$$f_r = \frac{c}{2\pi\sqrt{\mu_r \varepsilon_r}}\sqrt{\left(\frac{\rho_{nm}}{a}\right)^2 + \left(\frac{p\pi}{l}\right)^2} \qquad (1)$$

where f_r is the resonant frequency in Hz, c is the speed of light, μ_r and ε_r are the relative permittivity and permeability of the cavity space respectively, a and l are the cavity radius and height respectively, n, m and p are integers representing the standing wave mode numbers and ρ_{nm} is the mth root of the nth order Bessel function (either $J_n(x)$ for TM modes, or $J'_n(x)$ for TE modes). Equation (1) is used to geometrically tune the frequency at which the measurement will be performed. Utilizing different modes allows permittivity and permeability measurements at different frequencies [30] to provide some spectral information. The big advantage of MCP is that the measurement parameter is in the frequency domain, giving extremely high sensitivity when the resonant frequencies are in the GHz range. There are also small sample requirements (typical volumes of 200 mm^3) and for powders they can simply be filled into a tube with minimal preparation.

The main drawback of the MCP technique is that measurements can only be performed at spot frequencies defined by the cavity dimensions. The measurement is also volumetric, and thus an accurate determination of sample volume is required. Powders will have some air gaps and hence the measured quantity is not intrinsic unless the packing density is known. This is coupled with the uncertain depolarization factors associated with the specific shapes of the individual powder grains. Finally the definite identification of an unknown material is very challenging since many materials may have a similar absorption response at these frequencies. These weaknesses however can be addressed. The sparse data points in the frequency domain are not so much an issue since microwave relaxation phenomena such as Debye type behaviour is not expected as dipolar molecules do not exist. Frequency dependent data will only provide qualitative analysis on conduction mechanisms as described later. The solution to packing density and particle shapes is to quote an effective value of both permittivity and permeability which are less than the intrinsic values due to the volume of air gaps and field depolarization. Also, weighing of samples allows appropriate comparison measurements of materials with different densities. Finally, for the identification issue, in this application it is the characterization of a known precursor material and determination of a different product; a simple before and after experiment. The MCP technique in this respect is a much simpler and non-invasive method when compared to the aforementioned techniques although, they should be used as a complementary procedure.

III. Experimental methods

Fe_3O_4 powder (Bayoxide® E8712) initially exhibited a solid black colour consistent with Fe_3O_4. The particle sizes of this sample are quoted at approximately 0.3 μm. 500 mg of the powder was filled into an open vial and placed into a laboratory oven. Ten separate vials were prepared with each one annealed for 1 h at a different temperature, ranging from 60 to 300 °C, to vary the amount of oxidation of Fe^{2+} to Fe^{3+}. The resultant powder changed to a brown colour which was initially subjectively identified as γ-Fe_2O_3. The identification of this phase was carried out using XRD, XPS, VSM and MCP measurements. XRD was conducted using Cu Kα radiation at 1.545 Å from 10 to 80°. Offsets were removed and Gaussian curve fitting was applied at the relevant peaks in the data to match the materials. XPS spectra were collected using a Kratos Axis Ultra DLD system with a monochromatic Al Kα x-ray source operating at 144 W. Data was collected with pass energies of 160 eV for survey spectra and 40 eV for high resolution scans. Due to the magnetic nature of the samples under analysis, the system was operated in the electrostatic operation mode with an acquisition area of approximately 300 × 700 μm^2. Spectra were analysed using CasaXPS (v2.3.17) with sensitivity factors supplied by the instrument manufacturer. All spectra were calibrated to the C1s line for adventitious carbon at 284.8 eV. Magnetic hysteresis loops were measured at room temperature using a LakeShore® 7400 Series VSM System calibrated to a 3 mm nickel standard. The maximum applied field on the samples was 640 kA m^{-1}. The samples were dispersed at a fixed weight concentration of 10% inside a non-magnetic adhesive and left to dry in silicone moulds approximately 3 mm in width.

The microwave complex permittivity data was collected using our aluminium TM cylindrical cavity setup (inner diameter ø = 92 mm and height h = 40 mm) which uses a selection of TM_{0np} modes [30]. This cavity is designed to excite TM_{010}, TM_{011}, TM_{020}, TM_{021}, TM_{012}, and TM_{022} modes at frequencies of 2.5, 4.5, 5.7, 6.8, 7.9 and 9.4 GHz, respectively. The complex permeability was measured using our aluminium TE cylindrical cavity setup (ø = 95 mm, h = 40 mm) which uses a selection of

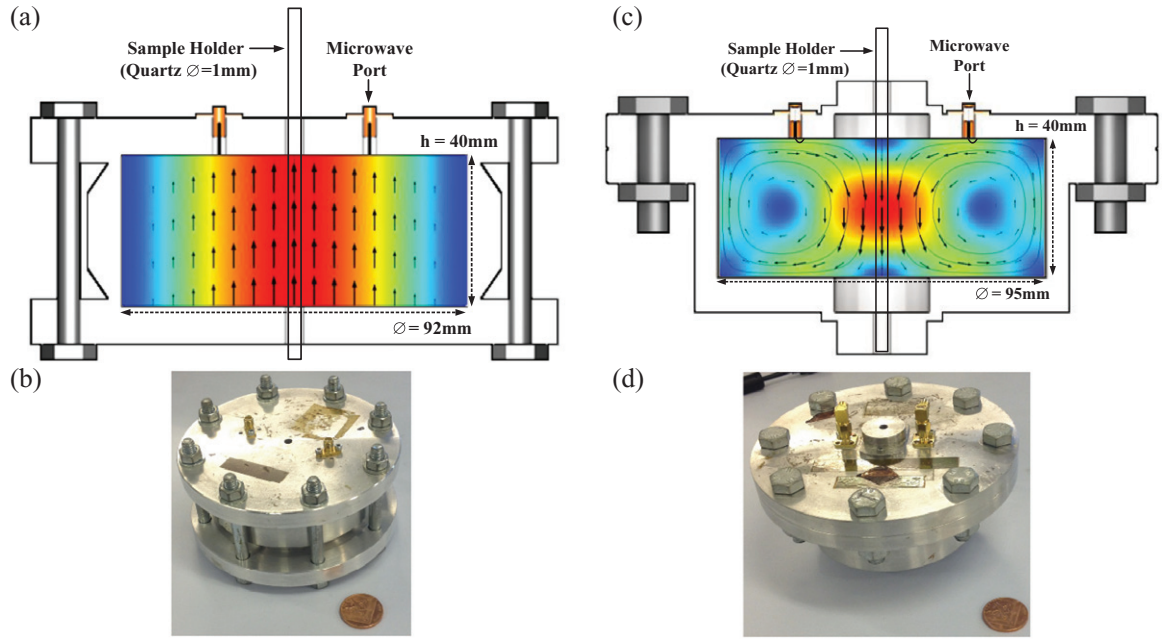

Figure 2. Cut section views and photographs of the cylindrical cavities used in this study. The permittivity measurement cavity shown in (a) and (b) is machined out of three blocks of aluminium (two cylindrical plates sandwiched onto an aluminium tube, held with steel bolts). The electric field distribution of the TM_{010} mode is shown in (a). The permeability measurement cavity shown in (c) and (d) is machined out of two pieces (one plate fastened onto an aluminium 'top hat' with steel bolts). The magnetic field distribution of the TE_{011} mode is shown in (c). Holes are drilled in both cavities for the antennas to inject microwaves and a hole is provided for the sample.

TM and TE modes [31]. This cavity is designed to excite TM_{110}, TE_{011}, TE_{021}, TE_{012} and TE_{022} modes at frequencies of 3.8, 5.4, 8.0, 8.4 and 10.2 GHz respectively. Both of these cavities are shown in figure 2. Microwave excitation and detection was provided by a Keysight Technologies PNA-L microwave network analyser using standard transmission measurements (i.e. S_{21}). Standard 3.5 mm flexible coaxial cables by Huber and Suhner were used to connect the PNA to SMA antennas on the cavity. Resonant trace data was logged using a program developed in National Instruments LabVIEW, which implements non-linear Levenberg–Marquadt curve fitting algorithms to a Lorentzian function to extract the parameters of resonant frequency, bandwidth and peak transmitted power.

The empty sample container was first placed at the sample location and measured to obtain the unperturbed frequency response. Quartz tubes ($ø = 1$ mm, $h = 100$ mm) were used due to their low microwave loss. The quartz tubes were then filled to a height such that the ends of the sample protrude from the cavity (at least 60 mm) to avoid macroscopic depolarization effects and placed on a vibrating stage for 5 min to allow the particles to settle in the tube. This forms the main source of error in that the differences in particle packing gives rise to different depolarization effects each time the tube is filled (and hence the effective complex permittivity and permeability may vary). The tubes were then placed in the cavity to conduct a perturbed measurement. Multiple S_{21} measurements were taken over a period of approximately 30 s at a sample rate of 1 Hz, with the average values of frequency and bandwidth used to calculate the permittivity/permeability and standard deviation used to provide random error (maximum of 5 kHz deviation, resulting in a measurement error of less than 1% for resonant frequency and 2% for bandwidth). The sample was placed with the field (either electric or magnetic) parallel to the sample tube, as shown in figure 2, to minimize any macroscopic depolarizing fields caused by the geometry of the sample container, though individual particle depolarization would still be present hence we quote effective and not intrinsic values. The effective relative dielectric permittivity, magnetic permeability and their equivalent losses were calculated using the simple, first order cavity perturbation equations [32]:

$$\alpha_{\mathrm{eff},1} - 1 \approx 2\frac{\Delta f}{f_0}\frac{V_\mathrm{e}}{V_\mathrm{s}} \tag{2}$$

$$\alpha_{\mathrm{eff},2} \approx -\frac{\Delta \mathrm{BW}}{f_0}\frac{V_\mathrm{e}}{V_\mathrm{s}} \tag{3}$$

where α_{eff} is the effective complex measurand, Δf and ΔBW are the differences in resonant frequency and bandwidth, respectively, from the unperturbed values, f_0 is the unperturbed resonant frequency, V_s is the volume of the sample within the cavity and V_e is the effective mode volume of the cavity. The mode volume is a scalar quantity calculated by integrating the total electromagnetic energy inside of the cavity and normalising it to the field at the sample location. Calculated values of each mode used in this study are all given elsewhere [30, 31]. The effective conductivity can also be extracted using the measured dielectric losses using:

$$\varepsilon_\mathrm{r} = \varepsilon_{1,\mathrm{d}}(\omega) - j\left[\varepsilon_{2,\mathrm{d}}(\omega) + \sigma_{\mathrm{AC}}(\omega)/\omega\varepsilon_0\right] \tag{4}$$

where $\sigma_{\mathrm{AC}}(\omega)$ is the frequency dependent AC conductivity, ω is the angular frequency and $\varepsilon_{1,\mathrm{d}}$ and $\varepsilon_{2,\mathrm{d}}$ are the polarization related contributions to the relative dielectric constant and losses, respectively. In most cases, either $\varepsilon_{2,\mathrm{d}}(\omega)$ or the

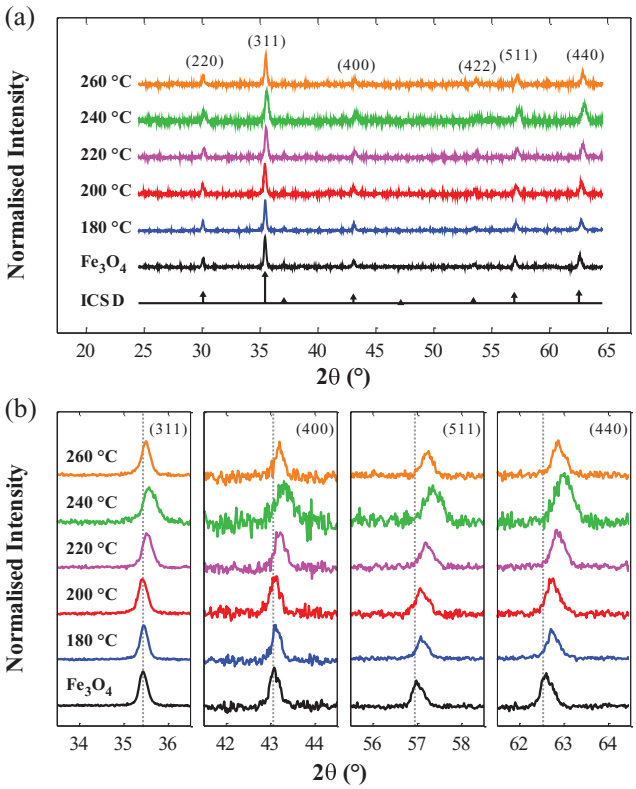

Figure 3. XRD patterns of the starting Fe_3O_4 powder and subsequent annealed powders (a). Close inspection of the relevant peaks (b) show upward shifts with increasing annealing temperature. The dotted lines show the angle positions of the ICSD pattern.

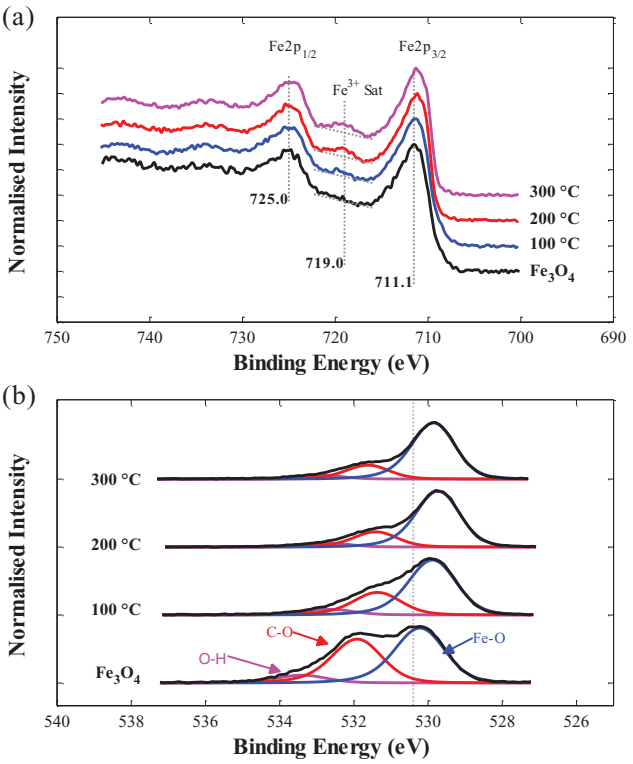

Figure 4. XPS patterns of the Fe2p (a) and O1s (b) core-level photoelectron spectra for Fe_3O_4 and subsequent annealing temperatures, both charge corrected to the C1s peak.

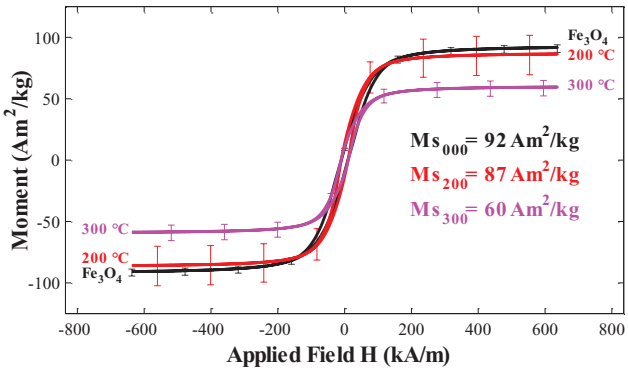

Figure 5. Hysteresis curves obtained using VSM of the starting Fe_3O_4 powder and annealed powders at 200 and 300 °C. Error bars given for three samples prepared separately and scaled based upon a powder weight concentration of 10%.

conducting term dominates (for example, in water $\varepsilon_{2,d}(\omega)$ dominates due to Debye relaxation caused by dipolar molecules whereas in semi-metallic powders it will more likely be conductivity related). Using these simple equations we can infer the dielectric, magnetic and conducting properties of powders.

IV. Results and discussions

IV.A. X-ray diffraction (XRD)

Diffraction patterns from 20 to 80° were collected, with data cropped to the significant peaks shown in figure 3. The diffraction patterns of the starting Fe_3O_4 powder and powders annealed around the inferred transition temperature from the microwave results were obtained. The pattern of the starting powder was matched to Fe_3O_4, with a strong (3 1 1) peak at approximately 35.4° accompanied with the (2 2 0), (4 0 0), (4 2 2), (5 1 1) and (4 4 0) planes of the cubic cell at 30.0, 43.1, 53.5, 57.0 and 62.6°, respectively. The same planes are evident for the annealed samples, but are shifted upward with increasing temperature indicating that structurally these materials have a spinel cubic lattice but with a changing lattice constant. The average calculated lattice constant from the higher diffraction angles of planes (5 1 1) and (4 4 0) yielded 8.39 Å and 8.36 Å for the starting Fe_3O_4 and the 260 °C annealed samples, respectively. (see supplementary material regarding instrumentation errors with the Inorganic Crystal Structure Database (ICSD) match, stacks.iop.org/JPhysCM/28/106002/mmedia). A trend in decreasing lattice constant is evident. The explanation behind the decreasing lattice constant may be due to the ionic radii of the Fe^{2+} and Fe^{3+} cations. Since Fe^{2+} cations have a larger ionic radius, the Fe–O spacing is greater. In γ-Fe_2O_3 the conversion of these cations to Fe^{3+}, along with the formation of vacancies, decreases the spacing which results in the shifted 2θ pattern. This result is congruent with the transformation to γ-Fe_2O_3 as given in the aforementioned literature. However, a convolution of two peaks for the (5 1 1) plane, as reported by Kim *et al* (2012), was not noticed in this material. This may be more of a consequence of the low resolution from the Cu Kα line, and hence the presence

Table 1. Summary of magnetic properties obtained from VSM measurements with errors over three different samples.

	0 °C (Fe_3O_4)	200 °C	300 °C
Hysteresis area $\times 10^3$ (J m^{-3})	34 ± 10	20 ± 30	8 ± 1
Coercivity, H_c (kA m^{-1})	9.7 ± 0.9	10.2 ± 0.5	11.1 ± 0.8
Magnetization, M_s (A m^2 kg^{-1})	92 ± 2	87 ± 9	60 ± 3
Remanence, H_r (A m^2 kg^{-1})	9 ± 2	13 ± 9	11 ± 4
Squareness, M_r/M_s	0.1 ± 0.03	0.2 ± 0.2	0.18 ± 0.09

of an intermediate phase may not be determined. Hence, from these results we can qualitatively conclude that structurally the phase change occurs at a temperature of at least 180 °C.

IV.B. X-ray photoelectron spectroscopy (XPS)

The high resolution XPS spectra are shown in figure 4. For the Fe_3O_4 starting material, the $Fe2p_{3/2}$ peak is centred at 711.1 eV and is ascribed to the convolution of both Fe^{2+} and Fe^{3+} signals in Fe_3O_4 [33]. Since Fe_3O_4 comprises of both Fe^{3+} and Fe^{2+}, the resultant peaks are a convolution of electron energies in both oxidation states and whilst the Fe^{3+}/Fe^{2+} ratio can be obtained through rigorous curve fitting, for this experiment only a qualitative identification of the γ-Fe_2O_3 phase is required.

Annealing reveals a change in the O1s spectra, with loss of organic contamination and the development of clear oxide and hydroxide peaks, the latter coming from exposure of the samples to air during transfer to the vacuum chamber for analysis. More importantly, the Fe2p region exhibits a slight downward shift in energy from 711.1 eV to 710.7 eV and the clear development of a satellite peak at around 719.0 eV is characteristic of the Fe^{3+} in γ-Fe_2O_3 and other forms of Fe_2O_3. Hence, this measurement shows that the phase change can be noticed, beginning at 100 °C and becoming complete by 300 °C.

IV.C. Vibrating sample magnetometry (VSM) and magnetic properties

Magnetic hysteresis curves of the annealed Fe_3O_4 samples are given in figure 5 with numerical calculations given in table 1. The calculated saturation magnetization for the starting Fe_3O_4 phase is 92 A m^2 kg^{-1}, which is the same as those reported in the literature [34] of approximately 92 A m^2 kg^{-1}. As the powder is annealed at higher temperatures, this value decreases to approximately 60 A m^2 kg^{-1} which is less than measured values [15] of 72 A m^2 kg^{-1} for γ-Fe_2O_3. The decrease in saturation is congruent with the change to the γ-phase and not the α-phase (since the saturation of hematite is two orders of magnitude less [34] and any signs of the α phase should appear in the XRD patterns due to the hexagonal structure). Coercivity after annealing has very little change; starting at approximately 9.7 kA m^{-1} and increasing to 11.1 kA m^{-1} (see table 1 for the associated errors). The significance of this value may infer the average particle size [35] and that it does not change by much during the phase transition since the particles retain their overall shape and simply

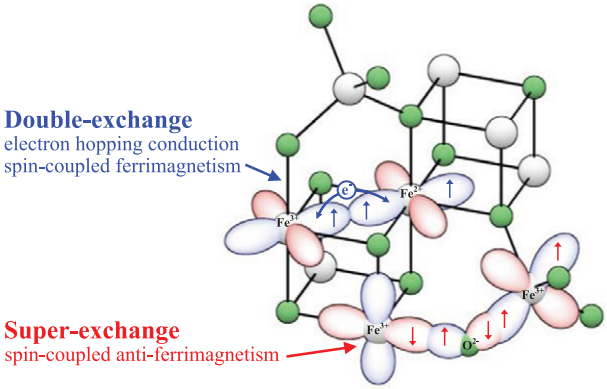

Figure 6. Conceptual representations of double and super-exchange interactions in Fe_3O_4 through d orbitals of Fe^{2+} and Fe^{3+} cations.

decrease in magnetic moment. The magnetic losses inferred by the integrated areas of the hysteresis curves show a large decrease with annealing temperature. Intrinsically relating this magnetic loss property to Fe_3O_4 and γ-Fe_2O_3 is not easy as it varies greatly with particle size and shape [36]. However, Fe_3O_4 has been shown to have larger magnetic losses than γ-Fe_2O_3 for micron sized particles [37].

The difference in magnetism between the two materials is a consequence of the cations in the inverse spinel lattice. For Fe_3O_4, ferrimagnetism exists through two main mechanisms, as given in figure 6. The first is the anti-ferromagnetic super-exchange interactions between the Fe^{3+}_{oct} and Fe^{3+}_{tet} cations through the O^{2-} anions [38]. The spin-up 5d electrons in the Fe^{3+}_{oct} couple with the overlapping 2p orbitals in the O^{2-} making them spin-down. The other 2p electron is thus spin-up which makes the Fe^{3+}_{tet} 5d electrons spin-down. Thus Fe^{3+}_{oct} and Fe^{3+}_{tet} are antiparallel and cancel out each other's unpaired spin magnetic moments. The second factor is related to the aforementioned double-exchange interaction [39]. The spin-down electron can only hop from Fe^{2+}_{oct} to Fe^{3+}_{oct} if the majority spins are the same. Hence they are coupled and aligned parallel. Therefore, all the Fe^{2+} cations contribute to the magnetic moment while all Fe^{3+} cations cancel each other out. However, in γ-Fe_2O_3 the conversion of 2/3 of the Fe^{2+}_{oct} to Fe^{3+}_{oct} balances some of the Fe^{3+}_{tet} cations but not all of them since the rest are turned into vacancies, resulting in a finite magnetic moment. When calculated, Fe_3O_4 has a larger magnetic moment [40] which is implied in table 1, thus providing more evidence that the phase change has occurred.

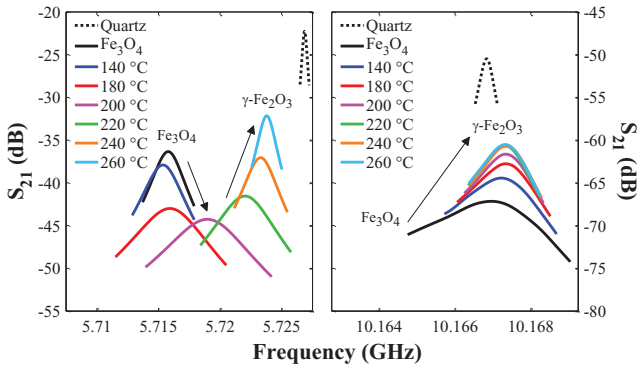

Figure 7. Selection of microwave cavity resonance traces, with the TM_{020} mode (left) used to measure permittivity and TE_{022} (right) for permeability.

IV.D. Microwave cavity perturbation (MCP)

MCP traces of two modes are given in figure 7. It is clear that the microwave properties of Fe_3O_4 change as it is annealed at different temperatures. This is shown by the changes in complex frequency, with a maximum in dielectric loss occurring at an annealing temperature of 200 °C. Taking the centre frequency and bandwidth of each trace of each resonant mode, the complex permittivity (thus conductivity) and permeability can be calculated.

The complex permittivity is given in figure 8. At temperatures below 180 °C both the effective dielectric constant and losses show minimal change. At higher temperatures, the dielectric constant decreases greatly while the losses increase to a peak and then decrease to effectively zero. There is also very little frequency dependence, as implied by all of the different resonant modes being superimposed upon one another. This consistency in the loss measurements implies an increasing effective conductivity with frequency, as calculated using (4). As more of the Fe^{2+} cations are oxidized to Fe^{3+}, the dielectric constant decreases, showing that the presence of Fe^{2+} cations provides a significant contribution to the polarization mechanism at microwave frequencies in Fe_3O_4 most likely due to the double exchange interactions explained later. With the assumption that only Fe^{3+} cations exist in the samples annealed above 200 °C as inferred by XPS, the permittivity measurements show that the contribution from the Fe^{3+} cations is much less without the mixed valence $Fe^{2.5+}$ at microwave frequencies.

A similar decrease is noticed in the losses, which reduce from approximately 0.4 to 0, as shown in figure 8. A large loss peak, however, is exhibited at around 200 °C, which intriguingly is not manifested in any of the other measurement techniques. This can be explained by a consequence of measuring a multiphase mixture in a microwave electric field if the difference in complex permittivity between the two phases is significant. Consider an air porous medium (ε_b) that consists of multiple spherical particles of radius b representing the Fe_3O_4 phase. After annealing, the powders are filled into the tube with a fraction of the Fe_3O_4 now converted to γ-Fe_2O_3. This can be represented as a spherical volume (ε_a) with radius a growing within the main volume. This volume is not actually growing inside the individual Fe_3O_4 particles since the oxidation process is expected to permeate from the

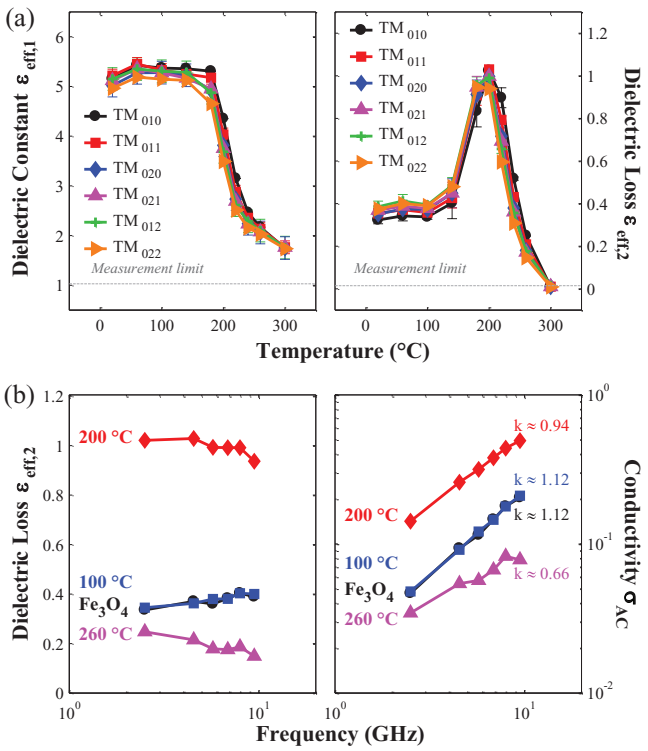

Figure 8. Calculated complex permittivity of annealed Fe_3O_4 samples using six different modes of the resonator as a function of annealing temperature (a) with error bars given as the standard deviation from the measurement of two separately filled powder tubes for a given annealed temperature and the dielectric losses and calculated effective AC conductivity as a function of frequency (b). Slope k for each is given for the model $\sigma_{AC}(\omega) \propto \omega^k$ explained later. The measurement limit is shown (calcuated from a 5 kHz deviation in frequency and bandwidth).

edges but represents a low loss volume growing within the bulk volume. The reason why the model has been considered in this way is because models for a lossy core and a low loss shell particle do not take into account the local field effects from other particles. In this model, the volume of the mixture remains the same, hence $a \leqslant b$. Eventually, all of the Fe_3O_4 phase disappears and the result is the γ-Fe_2O_3 phase or the low loss phase now occupies volume of the original particle so that $a \to b$. If this material is placed in an applied E-field (E_0), then the dipole moment per particle volume (P_i) of one of these inclusions can be described using the following formula [41]:

$$P_i = E_0 \frac{(\beta+2)(\alpha-1)\gamma^3 - (\alpha+2)(\beta-1)}{(2\beta-1)(\alpha+2) - 2(\beta-1)(\alpha-1)\gamma^3} \tag{5}$$

where $\alpha = \varepsilon_a/\varepsilon_b, \beta = \varepsilon_m/\varepsilon_a, \gamma = a/b$. In this instance we assume that the porous spaces are air (hence $\varepsilon_m = 1$). This formula can be incorporated into the well-known Maxwell-Garnett mixing law for multiple particles in a dielectric medium:

$$\varepsilon_{eff} = \varepsilon_m \left(\frac{1 + 2\delta_i P_i}{1 - 2\delta_i P_i} \right) \tag{6}$$

where δ_i is the volume fraction of the particles in the tube. In the case of a lossy particle with an increasing volume of a lossless dielectric, a loss peak can be exhibited at a certain volume fraction, as shown in figure 9. This loss peak only

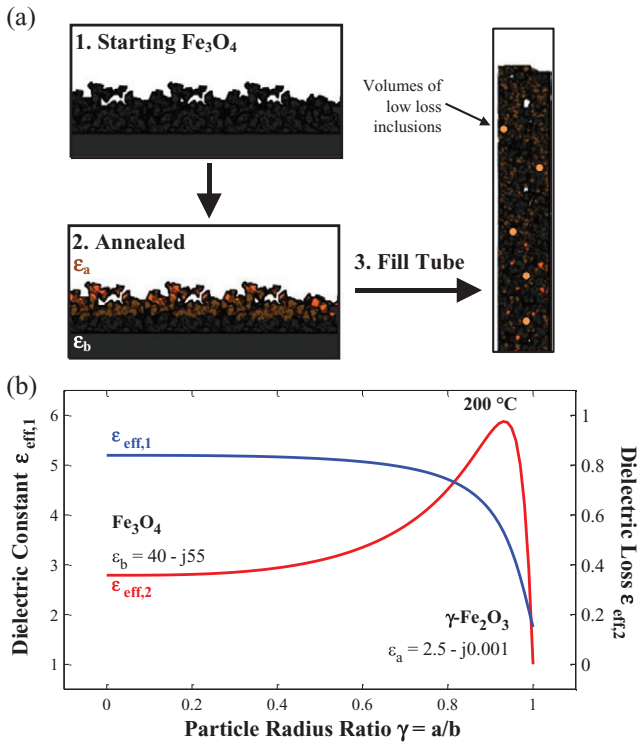

Figure 9. Abstract representation (a) of the annealing process resulting in a multi-phase mixture with a volume of the low loss phase inside the bulk mixture. Effective complex permittivity (b) is shown for a dielectric mixture ($\delta_i = 0.6$) as a function of particle radius ratio.

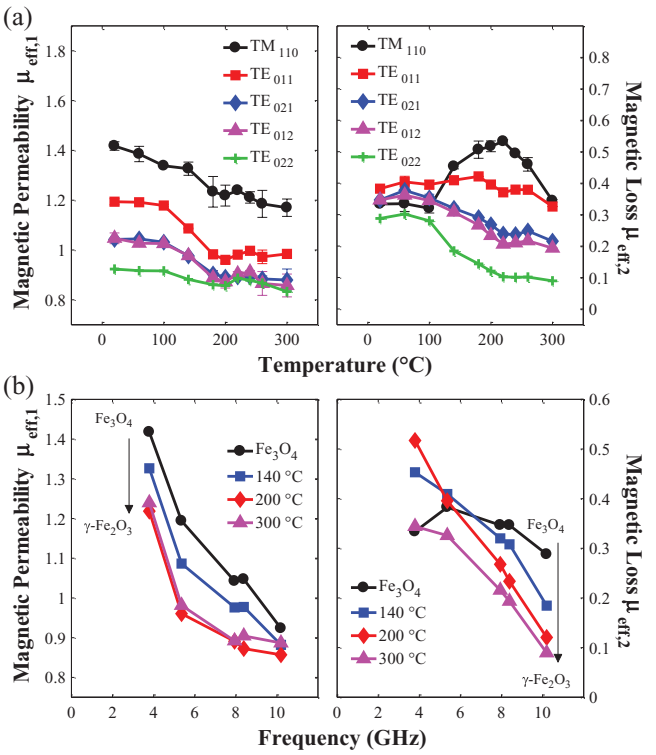

Figure 10. Calculated complex permeability of annealed Fe_3O_4 samples using five different modes of the resonator (a) as a function of annealing temperature with error bars given as the standard deviation of the measurement of two separately filled powder tubes for a given annealed temperature and as a function of frequency (b).

occurs, however, if the difference in permittivity between the materials is significant. Hence, microwaves maybe a very useful tool for looking at dramatic phase changes in materials and these materials may have excellent microwave absorbing properties at certain volume fractions.

Since Fe_3O_4 is a multi-valence oxide, it has a significant electrical conductivity which has been explained as a consequence of electron hopping from double exchange interactions through a chain of Fe^{2+}_{oct} and Fe^{3+}_{oct} cations [39]. This occurs because, being high spin [42], the cations only differ by one spin down electron, which is effectively delocalized due to minor overlapping between t_{2g} orbitals. In the transformation to γ-Fe_2O_3, 2/3 of the Fe^{2+}_{oct} cations are oxidized to Fe^{3+} while the remaining 1/3 diffuse of out of the lattice leaving behind vacancies [43]. The hopping dependent conductivity effectively explains why γ-Fe_2O_3 is an inferior conductor when compared to Fe_3O_4, as the conduction path through the cations is disrupted by the presence of vacancies and, assuming that the spin states in γ-Fe_2O_3 are high [16], there is no longer a delocalized spin-down electron. Hence, it is seemingly a case of one phase showing electron hopping conductivity and the other showing none. Now, as for the microwave methods, the hopping conduction mechanism will contribute to the loss as given by (4). The general model for hopping mechanisms in conductivity follows the Jonscher power law (JPL) [44]:

$$\sigma_{AC}(\omega) = \sigma_{DC} + A\omega^k \tag{7}$$

where σ_{DC} is the DC conductivity, A is a pre-exponential constant and k is the exponent of the power law. This law includes the restriction of $0 < k \leqslant 1$, while larger values indicate a super-linear power law (SLPL). The measured slopes are given in figure 8 where Fe_3O_4 gives a SLPL in this frequency range with an exponent k of approximately 1.12. For γ-Fe_2O_3 (annealed at 300 °C) the dielectric loss (and hence conductivity) is effectively zero at microwave frequencies. Taking the slopes of 200 and 260 °C annealed samples we find that the SLPL tends towards a regular JPL with k values of 0.94 and 0.66 respectively. Therefore, this implies that the SLPL characteristic in Fe_3O_4 at microwave frequencies may be a consequence of the Fe^{2+}_{oct} and Fe^{3+}_{oct} electron hopping mechanism [45]. Hence, the SLPL characteristic may also be a figure of merit for identifying the phase transition.

The complex permeability or magnetic permeability and losses are given in figure 10. From this study and previous work [31], the microwave magnetic permeability of Fe_3O_4 decreases with frequency while the losses have a broad peak over the 5.0–8.5 GHz range. As the powder is annealed, the overall magnetic permeability decreases with frequency, congruent with the VSM measurements. The losses, however, increase in the lower GHz range while decreasing in the higher range. This implies that the broad peak may have either disappeared, or has shifted to lower frequencies. The magnetic permeability is merely a tail of the natural ferromagnetic resonance peaks occurring at lower frequencies as given by the negative slopes. The greatest differences occur in the TE_{022}

Table 2. Potential resolution of the MCP measurements for Fe_3O_4 to γ-Fe_2O_3 ratio based on the effective complex permittivity.

Mode	Frequency (GHz)	$\frac{\Delta\varepsilon_{\text{eff},1,\text{max error}}}{\varepsilon_{(\text{eff},1,Fe_3O_4)} - \varepsilon_{(\text{eff},1,\gamma\text{-}Fe_2O_3)}}$ (%)[a]
TM_{010}	2.5	9
TM_{011}	4.5	12
TM_{020}	5.7	6
TM_{021}	6.8	9
TM_{012}	7.9	12
TM_{022}	9.4	10

[a] Resolution calculated by taking the largest measurable error caused by sample packing differences for each mode and dividing it by the difference in the effective dielectric constant between the starting powder and the powder annealed at 300 °C.

(10.2 GHz) mode in the losses, and in the permeability in the TE_{011} mode (5.4 GHz) as shown in figure 10. From the TM_{110} mode, the losses give a similar response as for the permittivity measurements, with a decrease in the real part and a large loss peak at 200 °C. Contrary to the permittivity measurements, the losses at 300 °C do not go to zero and are of similar values to the starting material. This may be explained by the fact that in Fe_3O_4 the dielectric and magnetic loss mechanisms are a consequence of the double-exchange interaction (i.e. electron hopping gives rise to conduction loss and the ferrimagnetism from coupled electron spins will have an associated magnetic alignment loss with an applied field). With the diffusion of Fe^{2+} cations and the formation of vacancies, the dielectric loss mechanism is eliminated but the magnetic mechanism is now due to the imbalance of tetrahedral Fe^{3+} and octahedral vacancies, or an absence of the super-exchange interaction (which caused the anti-ferrimagnetism in Fe_3O_4) and hence the losses are associated with this. The TE_{022} mode shows little changes in the real part but a large decrease in loss from 140 °C. The TE_{011} mode shows some change in the losses but larger changes in the real part, again occurring at 140 °C. The transition is somewhat less clear-cut than for the permittivity measurements, but when looking at the frequency dependent data the change can be clearly seen.

Qualitative information of the transition is apparent in all of the MCP measurements, however, it can be shown that quantification of the Fe_3O_4 to γ-Fe_2O_3 ratio can be achieved using the plateau responses given in the effective dielectric constant measurements and if the air gaps caused by the packing density are considered. However, measuring the density of the samples for a given mass and volume will require accurate determination of the fill height in the tube. In this case, there were no noticeable differences in mass but this was due to the very small sample volume and hence the associated measurement error of the mass was too large. Nonetheless, assuming that the starting and ending powders consist of 0% and 100% γ-Fe_2O_3 respectively, and the theoretical density of Fe_3O_4 and γ-Fe_2O_3 is similar at 5.2 and 4.8 kg m^{-3} respectively [46], the effective resolution ($\Delta\varepsilon_{\text{eff},1}$) in determining the concentration can be achieved from the maximum sample error given in figure 8(a). These values are given in table 2. Hence, for this particular MCP system and only with the assumption that the packing density is similar, the TM_{020} mode is potentially able to measure γ-Fe_2O_3 in concentrations of 6% only when it is mixed with Fe_3O_4 in these quartz tubes. This value is likely to increase if the packing density is significantly different amongst the samples but demonstrates the potential for MCP to extract this phase ratio.

V. Conclusion

We have shown that the MCP method is excellent for high-sensitivity, non-invasive materials characterization for the Fe_3O_4 to γ-Fe_2O_3 transition in annealed powders. We have also presented data from the standard methods of XRD, XPS and VSM techniques on these powders to corroborate the findings found with MCP. Each technique bears its own figure of merit for the characterization of the phase change. XRD results indicated the changing lattice constant from the upward shifting pattern in 2θ. XPS showed differences in binding energy caused by the different Fe cations at the surface of the material. Also Fe^{3+} satellite peaks associated mainly with the γ-Fe_2O_3 verified the change. VSM measurements provided hysteresis curves which showed that the starting material had a saturation magnetization very similar to Fe_3O_4, which decreased as the sample was annealed, again congruent with the change since γ-Fe_2O_3 is less magnetic. MCP measurements gave large frequency dependence for the effective permeability, with 3.8 and 10.2 GHz giving the most sensitive results, but with opposite behaviours of increasing and decreasing trends, respectively, with increased annealing temperature. Collectively looking over a broad microwave frequency range provides a better indication of the change qualitatively. Complex permittivity measurements, however, showed no frequency dependence but very large changes in both dielectric constant and loss. One cavity mode is sufficient for measuring the changes at microwave frequencies. The calculated conductivity of the powders showed a SLPL which may be due to the double-exchange hopping conduction caused by octahedral Fe^{2+} and Fe^{3+} cations. A loss peak was found at 200 °C, a consequence of field being focused at locations of inhomogeneity due to a multi-phase core-shell mixture. This insinuates that the phase change may occur around this temperature, with full transformation being reached at 300 °C. The γ-Fe_2O_3 phase has a smaller dielectric constant and negligible microwave losses when compared to Fe_3O_4. We conclude that the effects from Fe^{2+} cations can be probed very effectively using MCP and Fe^{3+} rich materials are likely to give minimal response. The presence of the loss peak in permittivity is a significant result for the applications of microwave absorber materials, as high loss tangents can be achieved through simple annealing of Fe_3O_4 at this temperature. This result shows that microwave dielectric measurements for all intents and purposes provide highly sensitive characterization of this oxidation process.

Acknowledgment

We acknowledge the financial sponsorship of Merck KGaA (Darmstadt, Germany) and the UK Engineering and Physical Sciences Research Council (EPSRC).

References

[1] Wang Z, Wu L, Zhou J, Cai W, Shen B and Jiang Z 2013 *J. Phys. Chem.* C **117** 5446
[2] Kong I, Ahmad S H, Abdullah M H, Hui D, Yusoff A N and Puryanti D 2010 *J. Magn. Magn. Mater.* **322** 3401
[3] Gama A M, Rezende M C and Dantas C C 2011 *J. Magn. Magn. Mater.* **323** 2782
[4] Du J H, Sun C, Bai S, Su G, Ying Z and Cheng H M 2011 *J. Mater. Res.* **17** 1232
[5] Bucak S, Yavuztürk B and Sezer A D 2012 *Recent Advances in Novel Drug Carrier Systems* ed A D Sezer (Rijeka: InTech) pp 165–200
[6] Spiers K, Cashion J and Gross K 2003 *Key Eng. Mater. Bioceram.* **254–256** 213
[7] Múzquiz-Ramos E M, Guerrero-Chávez V, Macías-Martínez B I, López-Badillo C M and García-Cerda L a 2015 *Ceram. Int.* **41** 397
[8] Li Z, Wei L, Gao M and Lei H 2005 *Adv. Mater.* **17** 1001
[9] Pankhurst Q A, Connolly J, Jones S K and Dobson J 2003 *J. Phys. D: Appl. Phys.* **36** R167
[10] Gendler T S, Shcherbakov V P, Dekkers M J, Gapeev A K, Gribov S K and McClelland E 2005 *Geophys. J. Int.* **160** 815
[11] Dinesen A R, Pedersen C T and Bender Koch C 2001 *J. Therm. Anal. Calorim.* **64** 1303
[12] Haneda K and Morrish A H 1977 *J. Phys. Colloq.* **38** 321
[13] Swaddle T W and Oltmann P 1980 *Can. J. Chem.* **58** 1763
[14] Agr R and September R 2002 *Geochim. Cosmochim. Acta* **66** 2801
[15] Serna C J and Morales M P 2004 *Surf. Colloid Sci.* **17** 27–81
[16] Grau-Crespo R, Al-Baitai A Y, Saadoune I and De Leeuw N H 2010 *J. Phys.: Condens. Matter* **22** 255401
[17] Fang M, Ström V, Olsson R T, Belova L and Rao K V 2012 *Nanotechnology* **23** 145601
[18] Chen T, Xu H, Xie Q, Chen J, Ji J and Lu H 2005 *Earth Planet. Sci. Lett.* **240** 790
[19] Espinosa A *et al* 2012 *Meas. Sci. Technol.* **23** 015602
[20] Chamritski I and Burns G 2005 *J. Phys. Chem.* B **109** 4965
[21] Jubb A M and Allen H C 2010 *ACS Appl. Mater. Interfaces* **2** 2804
[22] Hearne G and Pischedda V 2012 *J. Solid State Chem.* **187** 134
[23] Kim W, Suh C Y, Cho S W, Roh K M, Kwon H, Song K and Shon I J 2012 *Talanta* **94** 348
[24] Shebanova O N and Lazor P 2003 *J. Raman Spectrosc.* **34** 845
[25] de Faria D L A, Venâncio Silva S and de Oliveira M T 1997 *J. Raman Spectrosc.* **28** 873
[26] Tang B Z, Geng Y, Lam J W Y, Li B, Jing X, Wang X, Wang F, Pakhomov A B and Zhang X X 1999 *Chem. Mater.* **11** 1581
[27] Fukuchi T 2012 ESR techniques for the detection of seismic frictional heat *Earthquake Research and Analysis: Seismology, Seismotectonic and Earthquake Geology* (Rijeka: InTech) pp 317–40
[28] Noginov M M, Noginova N, Amponsah O, Bah R, Rakhimov R and Atsarkin V A 2008 *J. Magn. Magn. Mater.* **320** 228
[29] Weiss B P, Sam Kim S, Kirschvink J L, Kopp R E, Sankaran M, Kobayashi A and Komeili A 2004 *Earth Planet. Sci. Lett.* **224** 73
[30] Cuenca J A, Thomas E, Mandal S, Williams O and Porch A 2014 *Asia-Pacific Microwave Conf. (APMC)* (*Sendai, Japan*) pp 441–3
[31] Cuenca J A, Klein S, Rüger R and Porch A 2014 *44th European Microwave Conf. (EuMC)* (*Rome*) pp 128–31
[32] Cuenca J A, Thomas E, Mandal S, Williams O and Porch A 2015 *Carbon J.* **81** 174
[33] Allen G C, Curtis M T, Hooper A J and Tucker P M 1974 *J. Chem. Soc. Dalton Trans.* 1525
[34] Cornell R M and Schwertmann U 2003 *The Iron Oxides* (Weinheim: Wiley)
[35] Ma M, Wu Y, Zhou J, Sun Y, Zhang Y and Gu N 2004 *J. Magn. Magn. Mater.* **268** 33
[36] Elsherbini A A M, Saber M, Aggag M, El-Shahawy A and Shokier H A A 2011 *Magn. Reson. Imaging* **29** 272
[37] Spiers K M, Cashion J D and Gross K A 2004 *Key Eng. Mater.* **254–256** 213
[38] Gilleo M A 1958 *Phys. Rev.* **109** 777
[39] Rosencwaig A 1969 *Can. J. Phys.* **47** 2309
[40] Chirita M and Grozescu I 2009 *Chem. Bull. Politech. Univ. Timişoara* **54** 1
[41] Sihvola A H 1999 *Electromagnetic Mixing Formulas and Applications* (Illustrate) (London: IET)
[42] Bengtson A, Morgan D and Becker U 2013 *Phys. Rev.* B **87** 1
[43] Bowles J F W, Howie R A, Vaughan D J and Zussman J 2011 *Rock-Forming Minerals: Non-silicates: Oxides, Hydroxides and Sulphides* (London: Geological Society of London)
[44] Jonscher A K 1977 *Nature* **267** 673
[45] Lunkenheimer P and Loidl A 2003 *Phys. Rev. Lett.* **91** 207601
[46] Collinson D 2013 *Methods in Rock Magnetism and Palaeomagnetism: Techniques and Instrumentation* (Amsterdam: Springer)